# Intense keV IAP generation by orthogonally polarized multicycle midinfrared two-color laser fields

**Guicun Li (李桂存)[1,2], Yinghui Zheng (郑颖辉)[1,*], Zhinan Zeng (曾志男)[1,**], and Ruxin Li (李儒新)[1]**

[1]*Shanghai Institute of Optics and Fine Mechanics, Chinese Academy of Sciences, Shanghai 201800, China*
[2]*University of Chinese Academy of Sciences, Beijing 100049, China*
**Corresponding author: yhzheng@mail.siom.ac.cn; **corresponding author: zhinan_zeng@mail.siom.ac.cn*
Received March 14, 2017; accepted April 7, 2017; posted online May 2, 2017

We theoretically investigate the attosecond pulse generation in an orthogonal multicycle midinfrared two-color laser field. It is demonstrated that multiple continuum-like humps, which consist of about twenty orders of harmonics and an intensity of about one order higher than the adjacent normal harmonics, are generated when longer wavelength driving fields are used. By filtering these humps, intense isolated attosecond pulses (IAPs) are directly generated without any phase compensation. Our proposal provides a simple technique to generate intense IAPs with various central photon energies covering the multi-keV spectral regime by using multicycle midinfrared driving pulses with high pump energy in the experiment.

*OCIS codes: 190.2620, 020.2649, 320.2250, 320.7110.*
*doi: 10.3788/COL201715.071901.*

Attosecond (as) pulse generation, especially isolated as pulse (IAP) generation, has opened the route to the probe of the ultrafast processes and real-time observation of electron dynamics of molecules and atoms on an as time scale[1–5]. As the most powerful approach to generate as pulses, high-order harmonic generation (HHG), a highly nonlinear interaction of intense light with matter, has been extensively investigated during the past few decades[6–8]. HHG can be intuitively interpreted by the three-step model[9]. The outermost electron will be first tunneling ionized near the peak of the driving field, then accelerated, and finally recombines with the nucleus, emitting high-harmonic photons. For multicycle long pulses, the three-step process will be repeated in every half-optical cycle (OC), thus as pulse trains (APTs) are generated[10]. In order to generate an IAP, the harmonic emission must be confined within one half-cycle, leading to a single light burst. Present schemes for IAP generation basically involves carrier-envelope-phase stabilized few-cycle driving laser pulses[11], polarization gating (PG) technique[12], or multi-color laser waveform control[13–16]. The shortest IAP obtained in the experiment so far is 67 as covering 55–130 eV[17].

To date, HHG experiments have been widely performed by Ti:sapphire lasers at a wavelength of 800 nm, and phase-matching harmonics are limited to 150 eV. But in practical applications, such as biological imaging, the water window (280–540 eV) or keV X-ray pulses are of our special interest. To extend photon energies to this spectral range, midinfrared (MIR) laser fields have been used[18–21], which is primarily due to the cutoff law, $\hbar\omega_c = I_p + 3.17U_p$[9], where $I_p$ is the ionization potential of the target gas, and $U_p = 9.33 \times 10^{-14} I_L\ [\mathrm{W/cm^2}] \times (\lambda[\mu\mathrm{m}])^2$ is the acquired pondermotive energy of a free electron in the laser field. With the rapid development of the frequency down-conversion technique by optical parametric amplification (OPA) and optical parametric chirped pulse amplification (OPCPA), intense MIR pulses with the wavelength of up to 3.9 μms have been generated for HHG[19,20]. Using longer wavelength driving laser pulses combined with the extension of the phase-matching technique into the X-ray spectrum, bright coherent ultrahigh-order harmonics in the water window and keV X-ray regime have been generated[18,21]. Besides, soft X-ray as pulses covering the water window have been experimentally generated by 1.9 cycle 1850 nm MIR pulses[22,23] and the 1.7 μm 2 cycle MIR PG method[24]. However, the obtained harmonic yields are very low because of the unfavorable scaling of the single-atom response with laser wavelength[25,26]. In order to increase the efficiency, multi-color waveform synthesizing has been extensively used to loosen the requirement of driving pulse duration for IAP generation, decrease the pulse width of IAPs, and enhance harmonic yields. Previous studies focus on parallel multi-color schemes for IAP generation[13–16,27–29]. However, by adding an orthogonally polarized second pulse, the recollisions of free electrons can be manipulated 2D in atoms or molecules[30–35], and quantum trajectories will be preferentially selected[32–35], thus an IAP can still be generated[36,37]. In Ref. [36], the authors have theoretically investigated IAP in an orthogonally two-color (OTC) laser field, but they still used few-cycle pulses, which is quite difficult and will limit the pump energy in the experiment. In Ref. [37], the author has extended the driving pulse duration to more than ten OCs for IAP by superposing an orthogonally polarized multicycle chirped laser upon the driving pulse, and a single 410 as pulse can be obtained without any phase compensation, but this experimental alignment may be complicated, and the efficiency is low.

 

In this work, the generation of high-order harmonics (HHs) and IAPs in an OTC field consisting of an MIR fundamental pulse and its second-harmonic (SH) pulse is investigated. Compared with traditional 800 nm laser pulses, the cutoff can be easily extended to the X-ray spectrum by the MIR driving pulses. Besides, longer wavelength laser pulses can reduce the as chirp because the chirp scales as $\lambda^{-1}$[25], which is beneficial for short IAP generation. Moreover, our previous work showed that under the proper two-color delay, multiple electron trajectories can be reduced to a few or even a single recollision[38], and the inter-half-cycle interference effect becomes less pronounced even if driving pulses with a longer pulse duration are used[38–40]. Based the facts above, in this Letter, it is found that several quasi-continuum spectral humps that are stronger than other normal harmonics by about one order of magnitude, corresponding to intense IAPs as short as ~320 as, are directly generated without any phase compensation in our MIR-OTC field, which is not feasible in the 800/400 nm OTC field. Unlike conventional supercontinua, the semiclassical trajectory model[9,35] reveals that the quasi-continuum humps originate from the 2D control of electron–ion recollisions in our MIR-OTC field, thus providing a more advantageous technique to generate intense IAPs covering the water window or even multi-keV regime.

We simulate HHG in our MIR-OTC scheme by the strong-field approximation (SFA) model with the ground state depletion being considered[41]. The model atom in our simulation is He. The OTC field can be expressed as

$$E_s(t) = E_x f(t)\cos(\omega t)\overrightarrow{x} + E_y f(t+\tau)\cos[2\omega(t+\tau)]\overrightarrow{y}, \tag{1}$$

where $E_x$, $E_y$ represent the electric amplitudes of the fundamental and SH pulses polarized along the $x$ and $y$ directions, respectively. $f(t)$ is the Gaussian envelope, and $\tau$ is the two-color delay. According to Ref. [38], when the two-color delay is around zero, the number of recollisions will be greatly reduced. Therefore, $\tau$ is optimized to be zero in our simulation. The laser intensities of the fundamental and SH pulses are $6 \times 10^{14}$ and $1.2 \times 10^{15}$ W/cm$^2$, respectively. Both of the two pulses have the same duration (full width at half-maximum, FWHM) of 8 T (T is the OC of the fundamental pulse, the same hereafter). By using these simulation parameters, we have investigated HHG in the 800/400 nm IR-OTC field and 1800/900 nm MIR-OTC field, respectively, as demonstrated in Fig. 1, where (a) and (c) represent the harmonic spectra obtained by the 800/400 nm OTC field and the 1800/900 nm OTC field, respectively, (b) and (d) are the corresponding time frequency analyses of (a) and (c). It can be clearly seen from Figs. 1(a) and 1(c) that the cutoff is significantly extended when the 1800/900 nm MIR-OTC scheme is used. Besides, the harmonic spectrum is less modulated than that by the 800/400 nm OTC field. More surprisingly, multiple continuum-like spectral humps are generated near the cutoff. Each hump consists of about twenty orders of harmonics, and its intensity is about one order higher than its neighboring normal harmonic peaks, which corresponds to an intense IAP in the time domain.

According to Refs. [38–40], the harmonic spectrum can be interpreted as the interference effect of different quantum paths. Practically, only the trajectories whose dipole phase differences in each half-cycle are not significant can survive for the constructive interference and contribute to high-harmonic emissions[42]. For the multicycle OTC field, the phase difference of different trajectories for harmonic emission is proportional to $-(U_p/\omega) \propto \lambda^3$. Therefore, for the 800/400 nm OTC scheme, the phase difference for each half-cycle is very small, and many electron trajectories interfere constructively to contribute to HHG. This may be demonstrated in Fig. 1(b), where we can clearly see that there exist strong high-harmonic emissions in every half-cycle, leading to the constructive inter-half-cycle interference effect and well-resolved harmonic spectra. Conversely, in the 1800/900 nm MIR-OTC field, longer wavelength pulses will cause a large phase difference of different half-cycles, which will weaken the interference effect of different half-cycles, thus leading to less pronounced spectral modulation. This case can be illustrated by Fig. 1(d), where we can clearly see that intense continuum-like humps occur, corresponding to the cutoff region of each half-cycle, as denoted by the red circles (labeled as 1–4). For example, for the first hump that covers the 570th–590th (390–406 eV) harmonics, the strongest harmonic emission occurs at the return time of −2.685 T. Although there exist three other recombination times at −2.135, −1.625, and −1.115 T contributing to harmonic generation, they are too weak and have little influence on the interference effect of different quantum paths, thus leading to a quasi-continuum spectrum that has less pronounced spectral modulation.

To get a clearer insight of the underlying dynamics of the electron trajectories contributing to these humps,

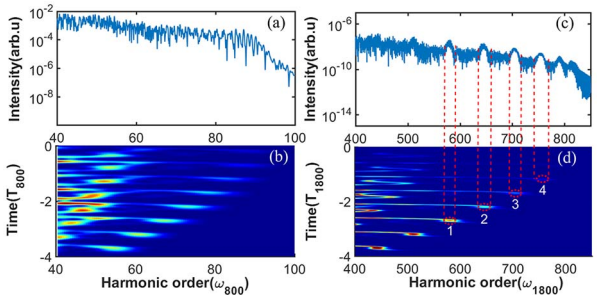


Fig. 1. (a) Harmonic spectrum obtained by the MIR 800/400 nm OTC field in the He atom. (b) The time frequency analysis of (a). (c) and (d) The same as (a) and (b), respectively, but for the MIR 1800/900 nm OTC field. In both cases the laser intensities are $I_\omega = 6 \times 10^{14}$ W/cm$^2$, (1800 or 800 nm), and $I_{2\omega} = 1.2 \times 10^{15}$ W/cm$^2$, (900 or 400 nm), the two-color delay is fixed at zero, and the fundamental and SH pulses have the same duration of 8 T. Note that diagrams (b) and (d) are plotted on the logarithmic scale.

we have also performed the semiclassical trajectory analysis in the 1800/900 nm MIR-OTC field[9]. Electrons are freed at the origin position with zero initial velocity at different ionization instants, and the 2D electron trajectories will be calculated by Newton's equation along the $x$ and $y$ directions, respectively[35]. It should be noticed that in the OTC field, the free electron does not necessarily need to exactly come back to the initial origin for HHG because of the quantum diffusion effect of the wave packet[41]. The returning wave packet can be assumed to be Gaussian and approximately expressed as

$$\varphi_d(r,t) = (\pi\sigma_t^2)^{-(1/4)} \exp\left[-\frac{(r-r_c)^2}{2\sigma_t^2}\right], \tag{2}$$

where $\sigma_t = [\sigma_0^2 + (t/\sigma_0)^2]^{1/2}$ and $r_c$ are the width and the center position of the diffused returning wave packet after excursion time $t$, respectively. $\sigma_0 = 4$ a.u. is the initial wave packet width[43]. The recombination probability is proportional to the spatial overlap between the diffused returning wave packet and the ground state wave packet, and given by

$$P_R \propto \int \varphi_d^*(r,t_r)\varphi_b(r)\mathrm{d}r. \tag{3}$$

In the long wavelength MIR-OTC driving field, the returning wave packet will diffuse seriously, and its width is much larger than that of the ground state wave packet $\varphi_b(r)$. Therefore, $\varphi_b(r)$ can be regarded as a delta function, and the integral of Eq. (3) is simplified as

$$P_R = \varphi_d(r=0,t_r) = \sigma_t^{-1/2} \exp\left(-\frac{r_c}{2\sigma_t^2}\right). \tag{4}$$

The harmonic yield is proportional to $|P_R|^2$, demonstrating that the HH yield decreases exponentially as the distance from the origin increases. Based on these discussions, we have calculated the electron trajectories at three different ionization instants around the electric field peak of $t = -3.5$ T, as shown in Fig. 2(a). The corresponding emitting photon energies are shown in Fig. 2(b). We only need to consider the return time within the half cycle from −3 to –2.5 T because the harmonic emission in other half cycles is very low, according to Eq. (4). $P_R$ is very low. In −2.5–2 T, however, the electron has a very long time to spread, and the width is very large, hence, the amplitude of the wave packet is very small, leading to very low recombination probability as well. From Fig. 2(d), we can see that the electron ionized at −3.4951 T gains kinetic energy and emits high harmonics with the highest photon energy of ~360 eV (blue line), thus making no contrition to the emission of the first hump 570th–590th (390–406 eV). However, when the electron is released at the later instant of −3.4870 T, it will return with the shortest distance (~0.2 a.u.) from the initial origin. We set a criterion that only the electron within 10 a.u. from the parent core has a substantial recombination

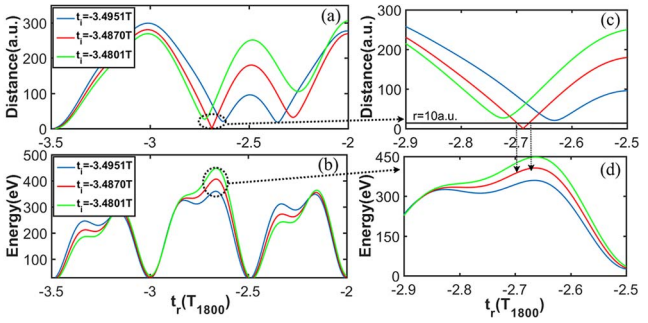


Fig. 2. (Color online) (a) Radial distance from the origin of the coordinate system as a function of the time after the electron is freed by the 1800/900 nm MIR-OTC field at −3.4951 T (blue line), −3.4870 T (red line), and −3.4801 T (green line), respectively. (b) The photon energy of the emitting high harmonics, corresponding to (a) as a function of different instants after ionization. (c) and (d) Enlarged diagrams of (a) and (b) in the time range from −2.9 to –2.5 T, respectively. The solid black line in (c) indicates that only the electron within 10 a.u. from the ionic core can emit strong high harmonics for a specific spectral range, as denoted by the arrows in (d). Laser parameters are the same as those in Figs. 1(c) and 1(d).

probability to emit high harmonics[30], as denoted by the solid line in Fig. 2(c). This will lead to strong harmonic emission with photon energies of 388–406 eV (red line), just corresponding to the first hump 570th–590th (390–406 eV), as indicated by the arrows in Fig. 2(d). In addition, the return time when the electron is closest to the origin position is −2.688 T, which is consistent with the emission time of −2.685 T obtained by the time frequency analysis in Fig. 1(d). Further, if the electron is freed at −3.4801 T, the electron will emit higher photon energies, exceeding the first hump (green line). Although the electron wave packet has a probability to recombine with the ground state wave packet and emits harmonics of the first hump, the distance from the origin is ~30 a.u. from Fig. 2(c), which is much larger than that of the electron released at −3.4870 T. In this case, the emission efficiency will be low. Therefore, the electron ionized around −3.4870 T has the maximum recombination probability and makes the largest contribution to emitting high harmonics corresponding to the first hump, while adjacent harmonics originate from the returns of the electrons that have a larger displacement from the ionic core, thus leading to a much weaker harmonic emission. This may explain why the each hump near the cutoff in each half-cycle is stronger than its neighboring normal harmonics. Similarly, other humps are generated in corresponding half-cycles in the same way. By selecting the appropriate hump with multi-layer metal-coated foil filters, an isolated as pulse radiation will be generated. The detailed results are shown in Fig. 3. It can be clearly seen from Fig. 3(a) that by superposing the harmonics from the 65th to 75th in the 800/400 nm OTC field, an as pulse with multi-peaks separated by a half-OC is generated. However, by selecting the appropriate hump in the 1800/900 nm MIR-OTC

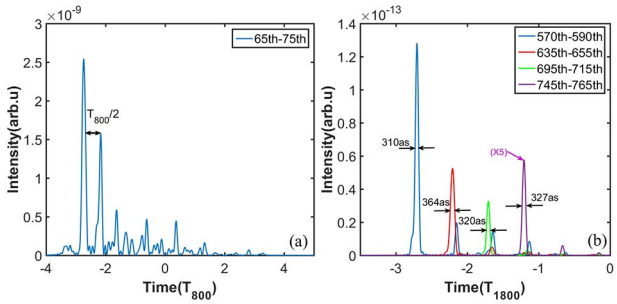


Fig. 3. (Color online) Time profiles of generated sub-cycle pulses by superposing the harmonics (a) from the 65th to the 75th order in the 800/400 nm OTC field and (b) from the corresponding spectral humps in the 1800/900 nm OTC field, respectively.

field, a clean ∼320 as pulse with a contrast ratio of more than 9:1 is directly generated without any additional phase compensation, as shown in Fig. 3(b), verifying that MIR-OTC driving laser pulses are more beneficial for IAP generation driven by multicycle pulses.

Moreover, we have compared the results obtained by our MIR-OTC field with that by the widely used parallel two-color field (PTC) and single-color field, as shown in Fig. 4. In both two-color schemes (parallel and orthogonal), simulation parameters are the same as those in Figs. 1(c) and 1(d). For the single-color 1800 nm field, the laser intensity is the sum of the two-color scheme, i.e., $I_\omega = 1.8 \times 10^{15}$ W/cm$^2$. We can clearly see from Fig. 4 that the cutoff is significantly reduced in the MIR-OTC scheme, compared with that by the single-color and PTC fields, which is consistent with previous results[34]. Furthermore, for the single-color 1800 nm field, the whole spectral region exhibits a severe modulation, indicating no IAP generation. For the PTC field, a multiplateau structure is generated, which may be resultant from the deep ionization of the ground state population[44]. For the OTC field, however, the intensity of the humps is about five times stronger than that in the PTC field,

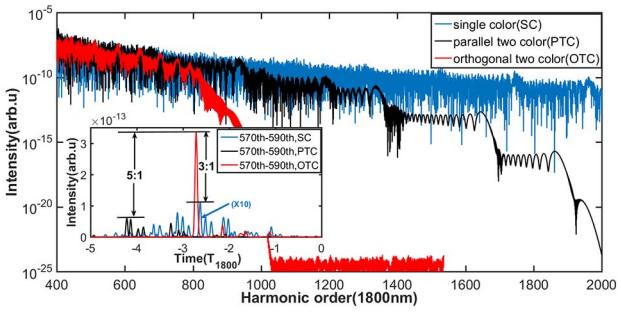


Fig. 4. (Color online) Harmonic spectra obtained by the single-color (blue line), PTC (black line), and OTC (red line) fields, respectively. In PTC and OTC schemes, simulation parameters are the same as those in Figs. 1(c) and 1(d). For the single-color 1800 nm field, the laser intensity is the sum of two-color schemes, $1.8 \times 10^{15}$ W/cm$^2$. The inset shows the time profiles by superposing 570th–590th harmonics (corresponding to the first hump in OTC field) generated by the three schemes.

which is consistent with the results in Ref. [33]. But Ref. [33] revealed that only the low-order harmonics in plateau were enhanced. In our work, however, we find that the harmonic yield of the humps near the cutoff can also be enhanced. The corresponding time profiles by superposing the 570th–590th harmonics (first hump in the OTC field) in three schemes are shown in the inset in Fig. 4, obviously demonstrating that only in the OTC field can a clean intense IAP be generated. Additionally, the intense IAP generated in our MIR-OTC scheme is about 5 times stronger than that in the PTC field and 30 times stronger than that in the single-color field. It is worth pointing out that although IAPs can be generated by selecting the multiplateau supercontinua in the PTC field, the efficiency is five orders lower than the humps.

Finally, we discuss the feasibility and generality of this MIR-OTC scheme. First, with the rapid development of the OPCPA technique, intense MIR pump pulses with a wavelength up to ∼4 μm are available in the laboratory[19,20]. Secondly, our MIR-OTC scheme can be directly applied for multicycle driving pulses, which will greatly relax the requirement for IAP generation and allow high-energy pump lasers. Thirdly, the optimum simulation parameters discussed in our work, such as two-color delay and driving pulse duration, are general for the MIR-OTC scheme. In our $\omega + 2\omega$ OTC scheme, the jitter between the two pulses can be neglected because the fundamental and SH pulses go through the same optical path, thus making the experimental setup more reliable and controllable. Another important issue is whether the humps still exist after considering the propagation effect. Our proposal is for intense IAP generation by multicycle high-power laser sources, which will be very loosely focused in the HHG experiment, thus the macroscopic effect can be significantly eliminated[44,45]. In such cases, the single-atom hump structure still applies in experimental conditions. Based on this, we directly extend the MIR-OTC scheme to 4000/2000 nm, for higher photon energy as pulse generation, and the harmonic spectrum is shown in Fig. 5. Other simulation parameters are the same as those in Fig. 1. It is obvious that multiple humps with different central photon energies are more clear and distinguishable. The inset in Fig. 5 shows that an isolated 360 as pulse can be directly generated by superposing 5993rd–6033rd harmonics, covering the 1857–1870 eV photon energy region, without any additional phase compensation. The results show the possibility of generating intense IAPs covering the multi-keV spectral regime by the MIR-OTC scheme.

In conclusion, the generation of HHs and IAPs in the MIR-OTC field is specifically investigated with the semiclassical model and the SFA model. By optimizing the two-color delay, it is found that multiple humps with different central photon energies are generated in the 1800/900 nm OTC field, corresponding to clean and intense IAPs as short as 320 as, which can be attributed to the 2D manipulation of the electron–ion recollision process and the suppression of the inter-half-cycle interference

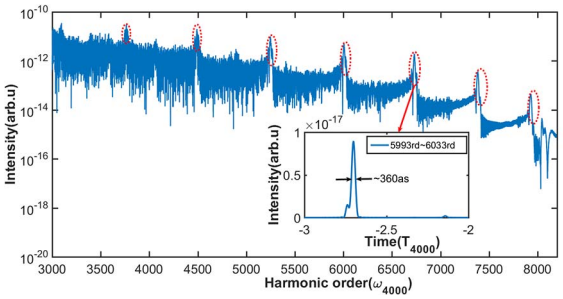


Fig. 5. High-harmonic spectrum in the 4000/2000 nm OTC field. Humps with different central photon energies are denoted by red ellipses. Other simulation parameters are the same as those in Fig. 1. The inset shows the time profile by superposing 5993rd–6033rd harmonics.

effect in the MIR-OTC field. In particular, the humps generated by the MIR-OTC field are stronger than their adjacent harmonics by about one order of magnitude. Although our simulation results are based on the single-atom responses, the hump structure is still feasible in future MIR-OTC experiments by a high pump energy laser system with loosely focused, long confocal parameters. Moreover, our MIR-OTC scheme, combined with phase-matching that is extended to the soft X-ray region, will greatly relax the requirement of driving pulse duration for IAP generation, substantially allow higher pump energy laser sources, and significantly enhance the as pulse intensity. By optimizing the MIR-OTC scheme and choosing appropriate gas media with loosely focused conditions, intense IAPs covering the multi-keV spectral range can be directly obtained by high-energy laser systems, which can be used for further scaling up the energy of the IAPs.

This work was supported by the National Natural Science Foundation of China (Nos. 11127901, 61521093, 11134010, 11227902, 11574332, 1151101142, 61690223, and 11274325), the Strategic Priority Research Program of the Chinese Academy of Sciences (No. XDB16), and the Youth Innovation Promotion Association of Chinese Academy of Sciences.

## References

1. M. Kitzler and M. Lezius, Phys. Rev. Lett. **95**, 253001 (2005).
2. H. Niikura, H. J. Wörner, D. M. Villeneuve, and P. B. Corkum, Phys. Rev. Lett. **107**, 093004 (2011).
3. P. B. Corkum and F. Krausz, Nat. Phys. **3**, 381 (2007).
4. F. Krausz and M. Ivanov, Rev. Mod. Phys. **81**, 163 (2009).
5. A. Baltuska, T. Udem, M. Uiberacker, E. Goulielmakis, C. Gohle, R. Holzwart, V. S. Yakovlev, A. Scrinz, T. W. Hänsch, and F. Krausz, Nature **421**, 611 (2003).
6. T. Ditmire, E. T. Gumbrell, R. A. Smith, J. W. G. Tisch, D. D. Meyerhofer, and M. H. R. Hutchinson, Phys. Rev. Lett. **77**, 4756 (1996).
7. P. Salières, A. L'Huillier, and M. Lewenstein, Phys. Rev. Lett. **74**, 3776 (1995).
8. T. Brabec and F. Krausz, Rev. Mod. Phys. **72**, 545 (2000).
9. P. B. Corkum, Phys. Rev. Lett. **71**, 1994 (1993).
10. P. Antoine, A. L'Huillier, and M. Lewenstein, Phys. Rev. Lett. **77**, 1234 (1996).
11. I. P. Christov, M. M. Murnane, and H. C. Kapteyn, Phys. Rev. Lett. **78**, 1251 (1997).
12. M. Ivanov, P. B. Corkum, T. Zuo, and A. Bandrauk, Phys. Rev. Lett. **74**, 2933 (1995).
13. Z. Zeng, Y. Cheng, X. Song, R. Li, and Z. Xu, Phys. Rev. Lett. **98**, 203901 (2007).
14. C. Jin and C. D. Lin, Chin. Phys. B **25**, 094213 (2016).
15. F. Li, G. L. Wang, S. F. Zhao, and X. X. Zhou, Chin. Phys. Lett. **32**, 014210 (2015).
16. P. C. Li, C. Laughlin, and S. I. Chu, Phys. Rev. A **89**, 023431 (2014).
17. K. Zhao, Q. Zhang, M. Chini, Y. Wu, X. Wang, and Z. Chang, Opt. Lett. **37**, 3891 (2012).
18. M. C. Chen, P. Arpin, T. Popmintchev, M. Gerrity, B. Zhang, M. Seaberg, D. Popmintchev, M. M. Murnane, and H. C. Kapteyn, Phys. Rev. Lett. **105**, 173901 (2010).
19. A. Andriukaitis, T. Balčiūnas, S. Ališauskas, A. Pugžlys, A. Baltuška, T. Popmintchev, M. C. Chen, M. M. Murnane, and H. C. Kapteyn, Opt. Lett. **36**, 2755 (2011).
20. T. Popmintchev, M. C. Chen, D. Popmintchev, P. Arpin, S. Brown, S. Ališauskas, G. Andriukaitis, T. Balčiunas, O. D. Mücke, A. Pugzlys, A. Baltuška, B. Shim, S. E. Schrauth, A. Gaeta, C. H. García, L. Plaja, A. Becker, A. J. Becker, M. M. Murnane, and H. C. Kapteyn, Science **336**, 1287 (2012).
21. E. J. Takahashi, T. Kanai, K. L. Ishikawa, Y. Nabekawa, and K. Midorikawa, Phys. Rev. Lett. **101**, 253901 (2008).
22. F. Silva, S. M. Teichmann, S. L. Cousin, M. Hemmer, and J. Biegert, Nat. Commun. **6**, 6611 (2015).
23. S. M. Teichmann, F. Silva, S. L. Cousin, M. Hemmer, and J. Bieger, Nat. Commun. **7**, 11493 (2016).
24. J. Li, X. Ren, Y. Yin, Y. Cheng, E. Cunningham, Y. Wu, and Z. Chang, Appl. Phys. Lett. **108**, 231102 (2016).
25. J. Tate, T. Auguste, H. G. Muller, P. Salières, P. Agostini, and L. F. DiMauro, Phys. Rev. Lett. **98**, 013901 (2007).
26. A. D. Shiner, C. T. Herrero, N. Kajumba, H. C. Bandulet, D. Comtois, F. Légaré, M. Giguère, J. C. Kieffer, P. B. Corkum, and D. M. Villeneuve, Phys. Rev. Lett. **103**, 073902 (2009).
27. H. Du, H. Wang, and B. Hu, Phys. Rev. A **81**, 063813 (2010).
28. W. Hong, P. Lu, Q. Li, and Q. Zhang, Opt. Lett. **34**, 2102 (2009).
29. X. Song, Z. Zeng, Y. Fu, B. Cai, R. Li, Y. Cheng, and Z. Xu, Phys. Rev. A **76**, 043830 (2007).
30. X. Gong, P. He, Q. Song, Q. Ji, H. Pan, J. Ding, F. He, H. Zeng, and J. Wu, Phys. Rev. Lett. **113**, 203001 (2014).
31. Q. Song, P. Lu, X. Gong, Q. Ji, K. Lin, W. Zhang, J. Ma, H. Zeng, and J. Wu, Phys. Rev. A **95**, 013406 (2017).
32. D. J. Hoffmann, C. Hutchison, A. Zaïr, and J. P. Marangos, Phys. Rev. A **89**, 023423 (2014).
33. I. J. Kim, C. M. Kim, H. T. Kim, G. H. Lee, Y. S. Lee, J. Y. Park, D. J. Cho, and C. H. Nam, Phys. Rev. Lett. **94**, 243901 (2005).
34. C. M. Kim, I. J. Kim, and C. H. Nam, Phys. Rev. A **72**, 033817 (2005).
35. L. Brugnera, D. J. Hoffmann, T. Siegel, F. Frank, A. Zaïr, J. W. G. Tisch, and J. P. Marangos, Phys. Rev. Lett. **107**, 153902 (2011).
36. Y. L. Yu, X. H. Song, Y. X. Fu, R. X. Li, Y. Cheng, and Z. Z. Xu, Opt. Express **16**, 686 (2008).
37. J. J. Xu, Phys. Rev. A **83**, 033823 (2011).
38. Y. Zheng, H. Diao, Z. Zeng, X. Ge, R. Li, and Z. Xu, Phys. Rev. A **92**, 033417 (2015).
39. P. Wei, J. Miao, Z. Zeng, C. Li, X. Ge, R. Li, and Z. Xu, Phys. Rev. Lett. **110**, 233903 (2013).
40. I. P. Christov, R. Bartels, H. C. Kapteyn, and M. M. Murnane, Phys. Rev. Lett. **86**, 5458 (2001).

41. M. Lewenstein, P. Balcou, M. Y. Ivanov, A. L'Huillier, and P. B. Corkum, Phys. Rev. A **49**, 2117 (1994).
42. J. H. Kim, H. J. Shin, D. G. Lee, and C. H. Nam, Phys. Rev. A **62**, 055402 (2000).
43. B. R. Galloway, D. Popmintchev, E. Pisanty, D. D. Hickstein, M. M. Murnane, H. C. Kapteyn, and T. Popmintchev, Opt. Express **24**, 021818 (2016).
44. W. Cao, P. Lu, P. Lan, X. Wang, and G. Yang, Phys. Rev. A **74**, 063821 (2006).
45. I. P. Christov, M. M. Murnane, and H. C. Kapteyn, Phys. Rev. A **57**, R2285 (1998).